

Stepwise Validated Finite Element Model of the Human Lumbar Spine

⁺Coombs D J, ^{*}Laz P J, ^{*}Rao M, ^{*}Smith S D, ⁺Bushelow M, ^{*}Rullkoetter P J

^{*}University of Denver, Denver, CO

⁺Synthes Spine, West Chester, PA

Abstract: Understanding the lumbosacral spine and the functional spinal unit (FSU) is essential in assessing the mechanics associated with normal spine function, spinal loading, degenerative disc disease (DDD), simulations of surgery as well as the impact of fusion, and total disc replacement (TDR). The lumbosacral spine and FSU comprise of bones and complex soft tissues such as intervertebral discs (IVD) and ligaments.

Prior studies have focused on the behavior of isolated structures, but the contribution of each structure to the overall kinematics of the spine needs to be further understood. The behavior of various structural conditions was determined by experimentally dissecting each ligament in a stepwise fashion until only the IVD remained, and applying loading conditions to the FSU. The FE model was validated through optimization to match the in vitro data for the various structural configurations, loading directions, and magnitudes.

Probabilistic studies based on these deterministic FE formulations are of great interest currently as model input parameters (such as properties of nucleus, annulus and facet, ligament stiffness and reference strain) have been characterized experimentally and contain substantial levels of variability.

Accordingly, the objective of the present study was to develop and validate an explicit FE model of the lumbosacral spine and the FSU L4-L5 using patient-specific in vitro data and to evaluate load-deflection characteristics, contact mechanics and efficiency of the FSU. Additionally, the objective was to create a probabilistic model to efficiently predict the performance of the FSU by incorporating disc and ligament material variability.

Keywords: Spine, Lumbar, Functional Spinal Unit, FSU, Disc, Kinematics, Biomechanics, Degenerative, DDD, Kinematics, Validation, Validate, Optimization, Probabilistic, Explicit, Rigid Body Kinematics, Contact

1. Introduction

Understanding the lumbosacral spine and the functional spinal unit (FSU) is essential in assessing the mechanics associated with normal spine function, spinal loading, degenerative disc disease (DDD), simulations of surgery as well as the impact of fusion, and total disc replacement. The FSU is comprised of bones and complex soft tissues, such as intervertebral discs (IVD), muscles and ligaments. Damage or degeneration of structures of the FSU is a common phenomenon

resulting in instability of the spine “(Oxland et al., 1991)”. Prior *in vitro* studies have focused on the behavior of isolated structures of the ligaments “(Chazal et al., 1985, Pintar et al., 1992)”, muscles “(Wilke et al., 1995)”, facet joints “(Wilson et al., 2006)”, IVD “(Polga et al., 2004)”, but the contribution of each structure to the overall kinematics of the spine is essential “(Panjabi et al., 1975)” and needs to be well understood. Heuer et al. performed *in vitro* testing to study the biomechanical effect of stepwise anatomy reduction for several loading magnitudes “(Heuer et al., 2007)”.

In the past, several FE models of the lumbosacral spine have been developed to simulate the behavior of normal spine mechanics “(Moramarco et al., 2010)”, instrumented spine mechanics “(Rohlmann et al., 2001)”, and the behavior of degenerated spinal structures “(Zander et al., 2004)”. Many models have been developed and validated with *in vitro* data from literature to quantify the overall mechanics of the lumbosacral segment “(Moramarco et al., 2010)”. However, no prior FE models have been created using patient-specific *in vitro* data involving a stepwise addition of structures resulting in a well performed calibration and structure validation. Additionally, a validated explicit FE formulation has advantages over an implicit FE formulation due to its efficiency in handling complex, changing contact conditions, the ability to evaluate either rigid or deformable body contact, and to reduce the analysis time to make optimization and probabilistic studies feasible.

Accordingly, the objectives of the present study were to develop and validate two patient-specific explicit FE models of the human lumbosacral spine. Stepwise addition of spinal structures, based on *in vitro* testing carried out at the University of Washington, was used to validate the healthy lumbosacral spine (none to mild disc degeneration) and the lumbosacral spine with mild to moderate disc degeneration. Analogous to the experimental testing, models were developed for individual FSUs and a multi-segment lumbar spine. Additionally, probabilistic simulations were employed and analyses were performed to predict performance incorporating disc and ligament material variability. The load-deflection characteristics, contact mechanics and efficiency of the FSUs were evaluated using deterministic and probabilistic approaches.

2. Methods

2.1 Specimen Selection and *In Vivo* Testing

A total of 10 specimens were selected and CT scans were obtained from the University of Washington. This data also included fluid pressure results from the discograms. The scans, along with the discogram results, were used to select the 2 best specimens which represented the desired spine conditions. The 2 specimens were Spine A (healthy - none-to-mild degeneration) and Spine B (mild-to-moderate degenerative changes), as summarized in Table 1. Four fiducial markers were placed in each vertebra to correlate the scanned geometry to the motion capture data.

Table 1. Selection of Two Lumbar Spines.

Spine	Age	Gender	Weight (lb)	Height (in)	Description
A	33	Male	130	70	Healthy adult lumbar spine with none-to-mild degeneration (Disc grade 1-2)
B	71	Male	267	68	Adult lumbar spine with mild-to-moderate degenerative changes (Disc grade 3-4)

Cadaveric in vivo testing was conducted at the University of Washington using a custom multi-axis spine motion simulator along with a Vicon 3D motion capture system. For each specimen, the intact multi-segmental (L1-Sacrum) spine was tested by fixing the sacrum and applying a 10 Nm pure moment to L1 in flexion/extension, lateral bending, and axial rotation. Combinations of pure moments were also applied including 7 Nm in flexion/extension with 7 Nm left and right lateral bending, 7 Nm flexion/extension with 7 Nm axial rotation, and 7 Nm lateral bending with 7 Nm axial rotation. In addition, a follower load of 450 N was applied during flexion extinction. Figure 1 shows the multi-segmental test setup. The spines were then dissected such that FSU's (L2-L3 and L4-L5) were tested. The FSU's were tested by removing the ligaments in a stepwise fashion. Table 2 summarizes the test steps performed during the protocol. During the initial intact step, the load was applied using load control to 10 Nm. The following steps were based on displacement control to the same angle that was achieved during the intact initial step (hybrid loading) because the FSU became less stable as structures were removed and would not be able to support the 10 Nm pure moment. Finally, the facets bony anatomy was removed and the only anatomy remaining was the IVD and the vertebral bodies. The hybrid loading was applied and a compression only load was applied in the axial direction to capture the stiffness of the IVD.

Table 2. FSU Test Protocol (L2-L3 and L4-L5).

Condition	Test Description	Tests performed
1	FCL, LFL, ITL, ALL, PLL, ISL, SSL (Intact)	FE, LB, AR ($\pm 10\text{Nm}$)
2	FCL, LFL, ITL, ALL, PLL, ISL (Remove SSL)	FE, AR (hybrid to intact ang. disp.)
3	FCL, LFL, ITL, ALL, PLL (Remove ISL)	FE, AR (hybrid to intact ang. disp.)
4	FCL, LFL, ITL, ALL (Remove PLL)	FE, AR (hybrid to intact ang. disp.)
5	FCL, LFL, ITL (Remove ALL)	FE, AR (hybrid to intact ang. disp.)
6	FCL, LFL (Remove ITL)	LB, LB, AR (hybrid to intact ang. disp.)
7	FCL, (Remove LFL)	FE, LB, AR (hybrid to intact ang. disp.)
8	facet cartilages (Remove FCL)	FE, LB, AR (hybrid to intact ang. disp.)
9	Disc only (Remove Facetets)	FE, LB, AR (hybrid to intact ang. disp.)
10	Disc only (Remove Facetets)	Axial Compression 1000 to 1500 N

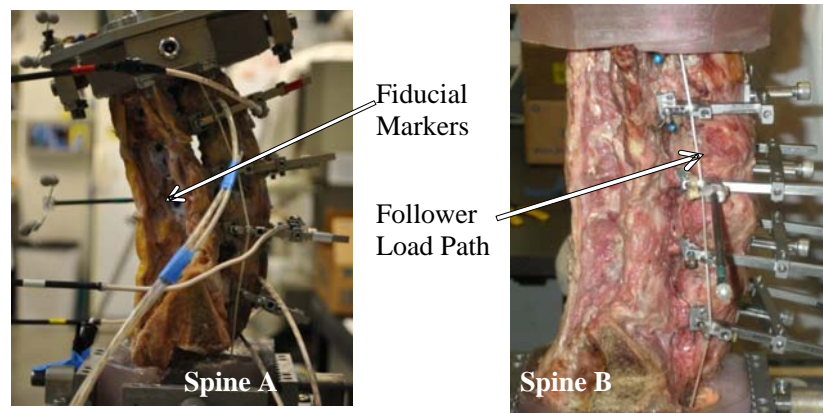


Figure 1. Multi-segmental test setup.

2.2 Model Development Workflow

After selecting the appropriate specimens, model development followed the workflow described in Figure 2. The CT scans were imported into ScanIP (simpleware, Exeter, UK) for reconstruction of bony geometry. The stereolithography (STL) file output from ScanIP was imported into Hypermesh (Altair Hyperworks, Troy, MI), where the task of mesh refinement and the addition of disc and ligament structures was completed. After all the components were placed in the appropriate locations, the model files were exported from Hypermesh and the analysis was performed in Abaqus/Explicit. Post-processing was performed using Abaqus/CAE and custom scripts were developed in Python.

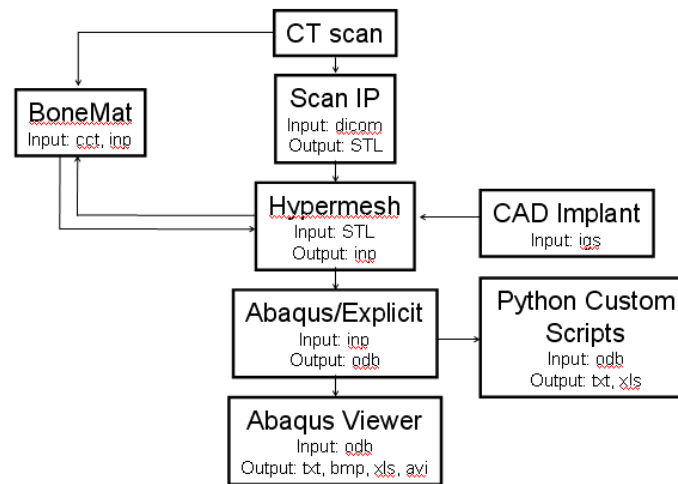


Figure 2. Model development workflow.

2.3 Finite Element Model Development

2.3.1 Vertebral Bodies

The 3D surface geometries from ScanIP were imported into Hypermesh. For computational efficiency during optimization, bones were considered rigid and represented by 3-noded triangular rigid elements (Element type=R3D3). Two millimeter radius fiducial markers were modeled and placed on the bone at appropriate locations based on the CT scans and cadaver images. Four markers were placed on each vertebral body and were meshed with 3-noded triangular shell elements (Element type=S3R). The reconstruction thus far was in the 'scan space'. After placement of the fiducial markers on the bones, the bony assembly with the markers was repositioned to match the 'experimental space'.

2.3.2 Ligaments

Seven of the load-bearing soft tissues structures crossing each of the FSU levels were represented by two-noded three-dimensional non-linear connector elements (Element type=CONN3D2), including the anterior and posterior longitudinal ligament (ALL, PLL), supraspinous and

interspinous ligament (SSL, ISL), intertransverse ligament (ITL), facet capsular ligament (FCL) and ligamentum flavum (LFL), as shown in Figure 3. The ALL was represented as 7 springs in series and 26 springs in parallel. The PLL was comprised of 7 springs in series and 26 springs in parallel. The SSL was represented as 1 spring in series and 1 spring in parallel. The ISL was represented as 1 spring in series and 5 springs in parallel. The ITL was represented as 1 spring in series and 2 springs in parallel. The FCL was represented as 1 spring in series and 4 springs in parallel. The LFL was represented as 1 spring in series and 3 springs in parallel. The ligament attachment sites were primarily based on the dissection performed after testing and confirmed with literature descriptions “(Panjabi et al., 1991)”. Ligament mechanical properties (stiffness and reference strains) were adjusted to match reported laxity profiles under various loading conditions (flexion, extension, lateral bending and axial rotation) performed during testing.

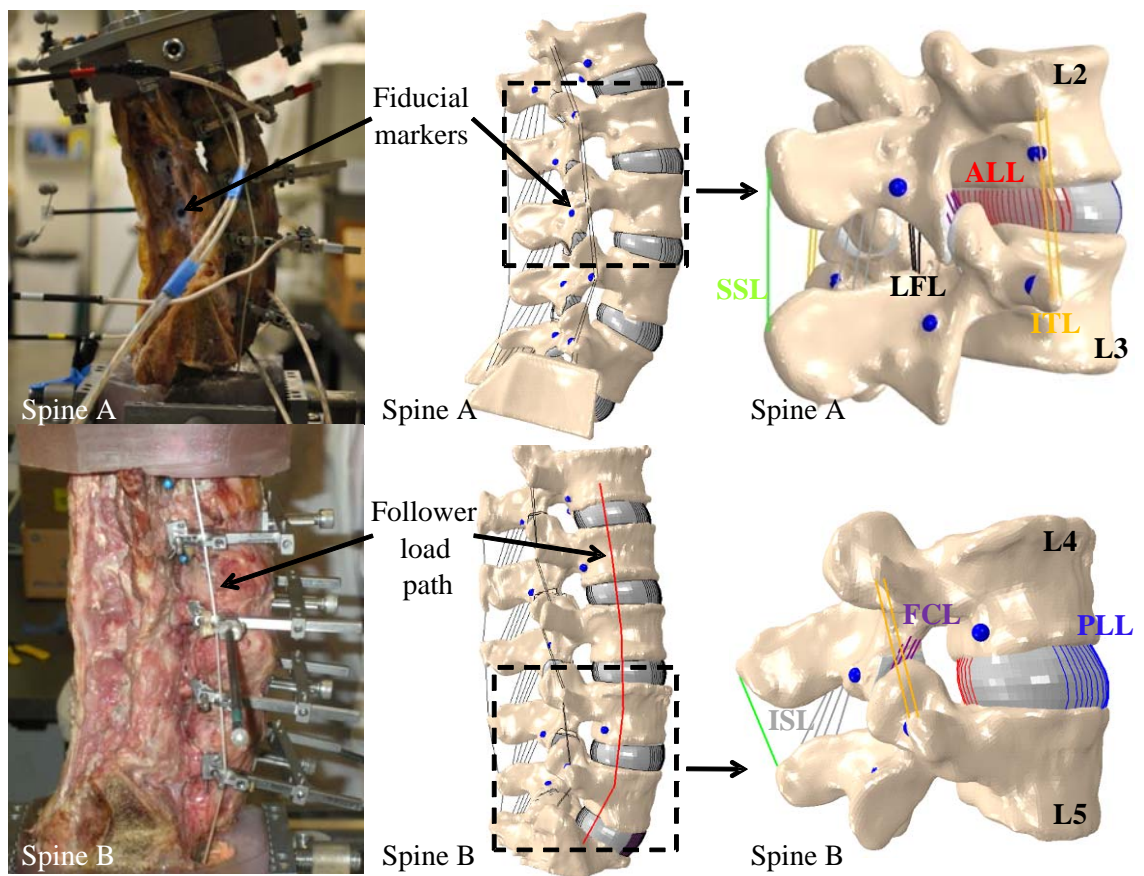


Figure 3. Spine A and Spine B - Cadaveric setup with follower load fixtures and cables. Subject-specific finite element model with the follower load path. Ligamentous representation of the Spine A FSU L2-L3 and Spine B FSU L4-L5.

2.3.3 Facet Joints

While the framework allows representation of the facet joint as rigid or deformable, the articulating facet surfaces were considered rigid represented by 8-noded hexahedral elements (Element type=C3D8R) to improve computational efficiency, as shown in Figure 4. For all the analyses, the facet contact pressure-overclosure relationship was defined by a previously verified relationship that matched the rigid and deformable results. The contact maps computed during FE analysis were closely matched with the Tekscan data measured during the experiment.

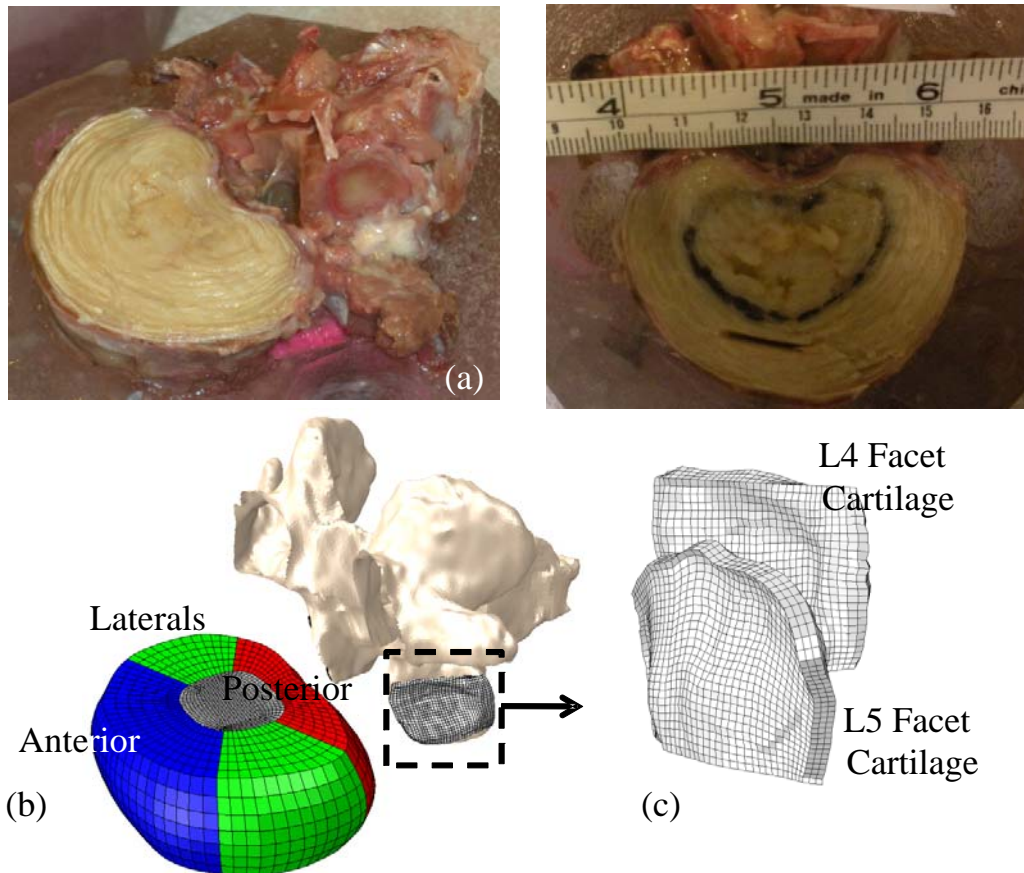


Figure 4. (a) Dissection of the IVD and marking of AF-nucleus region. (b) Hex mesh representing the AF and its three regions (c) Hex mesh of the articulating facet cartilages.

2.3.4 Intervertebral Discs

Based on the dissected geometry of the IVD, as shown in Figure 4a, the annulus fibrosus (AF) comprised of three major regions (anterior, posterior and laterals) modeled as 8-noded hexahedral

elements (Element type=C3D8R) and an 8 noded fluid-filled membrane representing the nucleus pulposus (Element type= SFM3D4R), as shown in Figure 4b. The regions of the AF were represented as anisotropic hyperelastic (Holzapfel) with C_{10} , D , k_1 , k_2 and $kappa$ being the material constants. Uniaxial tensile tests were simulated with specimens from different regions of the AF to match the literature micro behavior of the AF, as shown in Figure 5. Uniform rectangular geometry of the AF was modeled according to the measurements reported in literature, as summarized in Table 3. A total of 6 circumferential, 2 axial and 2 radial specimens, as shown in Figure 5, were developed in Abaqus/Standard from dimensions given in Table 3. These values were used either as a starting point for the optimization routines or to verify if the optimized values approximately matched literature values.

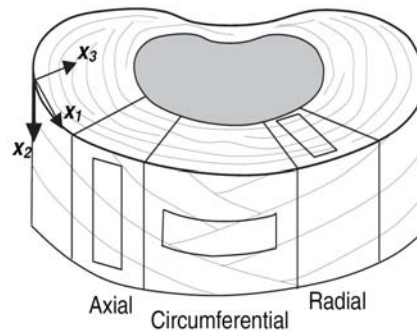


Figure 5. Regions and specimen orientation of the AF

Table 3. Measurements of the rectangular specimens.

Reference	Length [mm]	Width [mm]	Thickness [mm]
Ebara et al., 1996	3.7	4.4	2.3
Guerin et al., 2007	9.55 ± 1.06	2.83 ± 0.32	1.94 ± 0.38
Holzapfel et al., 2005	10.00 ± 2.3	3.0 ± 1.5	0.4 ± 0.06
Wagner et al., 2004	10	14.7	1.57

The fibers were aligned at 30° and 150° to the horizontal. As a starting point, the ground substance was modeled with predefined material constants C_{10} , D , K_1 , K_2 and $kappa$. Uniaxial analyses were performed using Abaqus/Standard. In the uniaxial simulations, one end of the specimen was fixed and loading in the form of force or displacement was applied to the other end at a constant rate.

Force-displacement data was extracted from each analysis using Abaqus/CAE and all data matching procedures were performed using Isight through minimization of the sum of squared errors in force-deflection procedures. The material constants C_{10} , D , K_1 , K_2 and $kappa$ were optimized based on the uniaxial experimental data “(Fujita et al., 1997, Guerin et al., 2007)”.

On completion of individual direction data fitting, multiple loading direction data were used to calibrate the combined behavior of the ground matrix and fibers. For example, for the anterior outer site, simultaneous data matching was done for circumferential and axial direction to obtain one set of anisotropic hyperelastic materials.

2.4 FSU Analysis

2.4.1 Deterministic FE Analysis (Intact and Stepwise Structural Addition)

As discussed in section 2.1, the FSU *in vitro* cadaver testing protocol followed a stepwise reduction of structures. In contrast, to validate the FSU finite element models, Abaqus/Explicit analyses were performed using a stepwise addition of structures. The approach started with the most basic configuration of the bones separated by the IVD, also called ‘disc only’. The facet cartilages were then added in the model, followed by the facet capsules (FCL), ITL, ALL, PLL, LFL, ISL, and SSL. Table 4 summarizes how the structures were added and which tests were performed.

Pure moment analyses in the principal axis – Flexion-Extension (Flex-Ext), Lateral bending (LB), and axial rotation (AR) were simulated in force control to a moment limit of 10Nm for the intact configuration. In the case of the “hybrid” analyses, the analyses were carried out in displacement control to the maximum angle limit recorded during the specimen’s intact configuration. Except for the intact configuration analysis, the inferior bone was kept fixed and displacement was applied to the fiducial markers modeled on the superior bone to reproduce the hybrid tests. The finite element analysis was repeated after the addition of each spinal structure to evaluate the contribution of the sectioned structures to the overall stability of the segment. Reaction moments from the analysis were compared to the moment measured during the testing. In addition to pure moments, compressive tests were simulated on three FSU’s where the load was ramped up to 1000N to obtain a relationship between load-displacement and characterize the stiffness of the IVD.

Table 4: Sequential structural addition protocol used for FE analysis.

Condition	Test Description	Tests performed
1	Disc only	FE, LB, AR (hybrid to intact ang. disp.)
2	Add facet cartilages	FE, LB, AR (hybrid to intact ang. disp.)
3	Add FCL and LFL	LB, LB, AR (hybrid to intact ang. disp.)
4	Add FCL, LFL, and ITL	FE, AR (hybrid to intact ang. disp.)
5	Add FCL, LFL, ITL, and ALL	FE, AR (hybrid to intact ang. disp.)
6	Add FCL, LFL, ITL, ALL, and PLL	FE, AR (hybrid to intact ang. disp.)
7	Add FCL, LFL, ITL, ALL, PLL, and ISL	FE, AR (hybrid to intact ang. disp.)
8	Add FCL, LFL, ITL, ALL, PLL, ISL, and SSL	FE, AR (hybrid to intact ang. disp.)
9	Intact	FE, LB, AR (\pm 10Nm)

2.4.2 Optimization

In a given analysis, twelve to twenty five input parameters were included in the optimization based on the configuration that was being evaluated: C_{10} , K_1 , K_2 and $kappa$ for three regions of the AF, seven ligament stiffness, three translations (along X, Y, Z axis) and three rotations (about X, Y, Z axis) of the facet cartilage. Using literature values to define initial and upper and lower bounds for stiffness, input parameters were perturbed with the adaptive simulated annealing global optimization algorithm adapted in Isight to minimize the root mean squared differences between the model-predicted and experimental force-deflection or reaction moment-time curves.

2.5 Intact Multisegmental Analysis

For the L1-Sacrum analysis, the sacrum was fully constrained with a 450N follower load (FL) (only during flexion-extension), and a pure moment of 10Nm was applied to L1. A manual

optimization of the FL path was performed to minimize the intervertebral rotations after FL application. Similar to the FSU optimization, the input parameters were perturbed using Isight with the adaptive simulated annealing algorithm to minimize the RMS differences between the model-predicted torque-rotation curves. The optimized input parameters for the FSU's were used as the initial values.

3. Results

3.1 Annulus Fibrosus Uniaxial Test

A uniaxial tensile test was simulated for the various regions of the AF. The optimized values for the anisotropic hyperelastic material constants were predicted using an optimization routine within Isight. The material properties for their respective regions are shown in Figure 6. Excellent agreement was seen between the experimental data (shown as data points) and the model with optimized parameters (shown as curves).

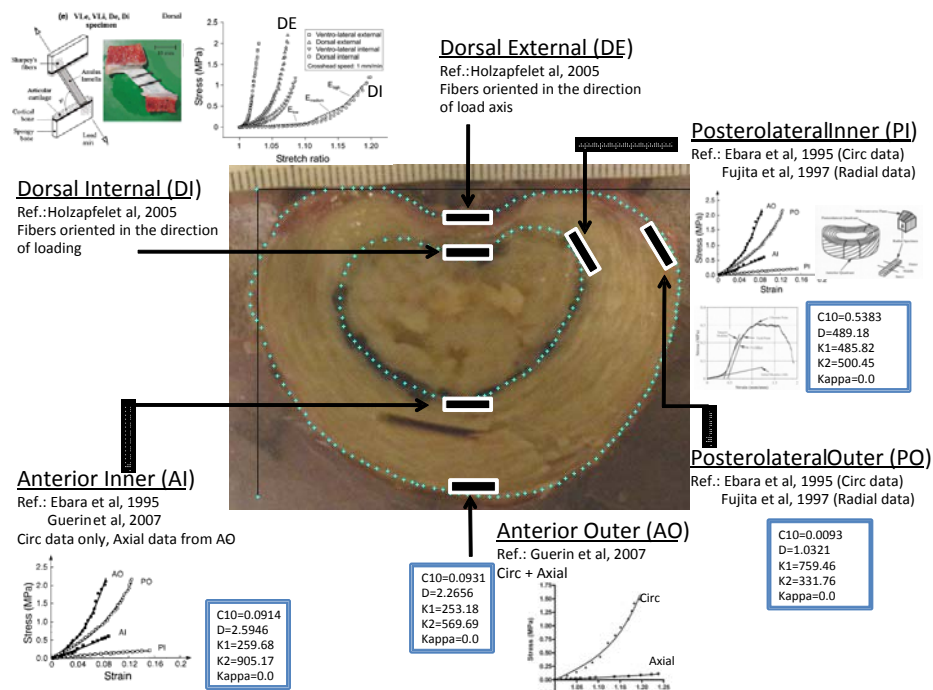


Figure 6. Optimized material constants for AF uniaxial tensile test.

3.2 FSU Analysis

3.2.1 Axial Compressive Stiffness of the Intervertebral Disc

Compressive load was applied to three FSUs and following the optimization process, the force-displacement results closely matched the experimental data shown in Figure 7. In the FE model, compressive force of 1000N caused displacements of 1.10, 1.33, and 0.98 mm for Spine A (L2-L3), Spine A (L4-L5), and Spine B (L4-L5) respectively. IVD for Spine B was slightly stiffer than the healthy Spine A at both levels, which was in line with the experiment.

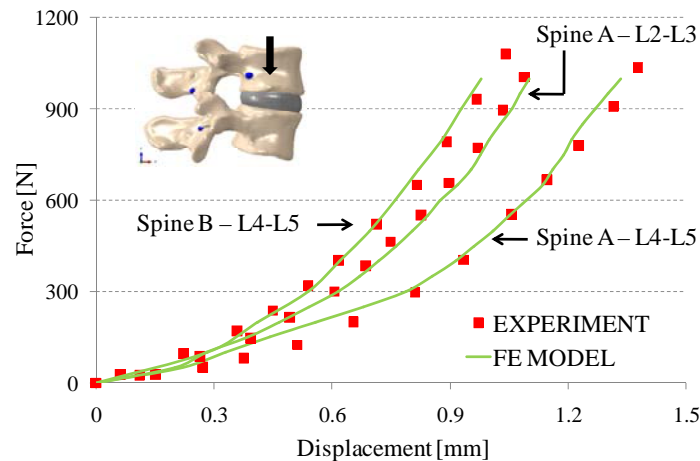


Figure 7. IVD axial compression optimization results.

3.2.2 Isight Optimization Based on Data Matching Following Resection Protocol

Optimization results, based on Isight, for Spine B FSU L4-L5 are shown in Figures 8, 9, and 10 for flexion-extension, lateral bending and axial rotation with various levels of intact structures that correspond to the experiment. The reaction moment was predicted as a function of time to perform optimization on the structure properties to reproduce the collected experimental data. Reaction moment-time behavior in Figure 8 corresponded to disc only, and results in Figure 9 were for disc and facets. The results of all structures intact are shown in Figure 10. Similar results were generated as each ligament was added according to Table 4, however only representative results are presented in Figures 8, 9, and 10. Similarly, only results from Spine B are presented, but optimization results were also generated for Spine A. As expected with the model tuning, the FE model prediction was in good agreement with the experiment.

In disc only tests, shown in Figure 8, there was less resistance offered by the disc; hence lower moments (~0.4 to 5.5 Nm) were necessary to achieve the rotation of the intact FSU. In comparison, moments of ~10 Nm were required to achieve the same rotation due to the presence of almost all structures of the functional spinal unit, as shown in Figure 10.

Another way to represent the results of the optimized intact model was to graph the torque-rotation curves. Representative motions of the vertebral bodies for Spine B, L2-L3 and L4-L5, are shown in Figure 11.

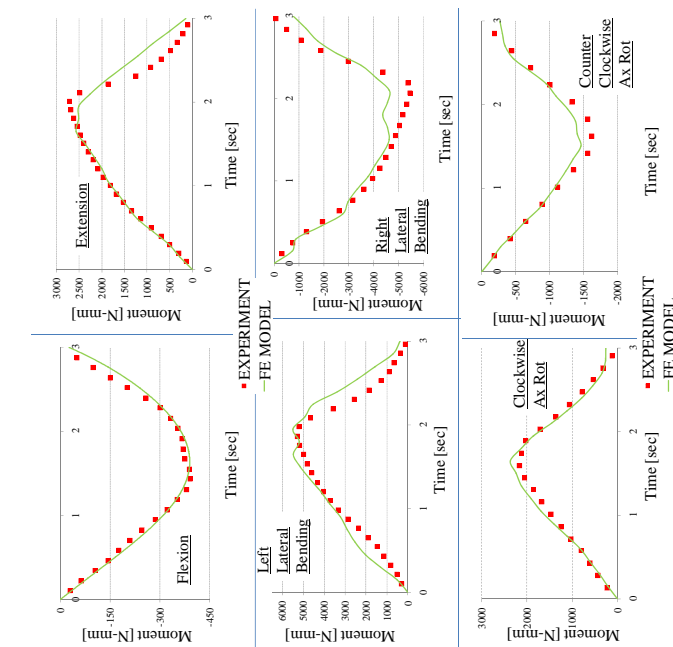


Figure 8. Reaction moment vs. time, disc only, spine B.

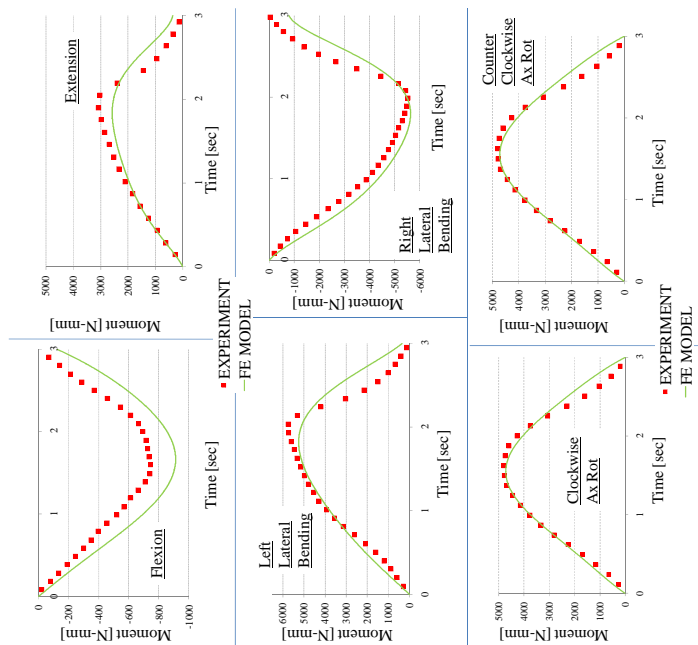


Figure 9. Reaction moment vs. time, disc + facets, spine B.

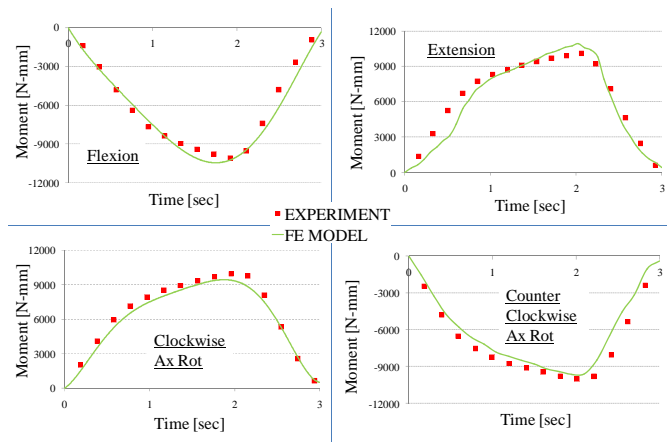


Figure 10. Reaction moment vs. time, disc + facets + FCL + LFL+ ITL + ALL + PLL + ISL, spine B.

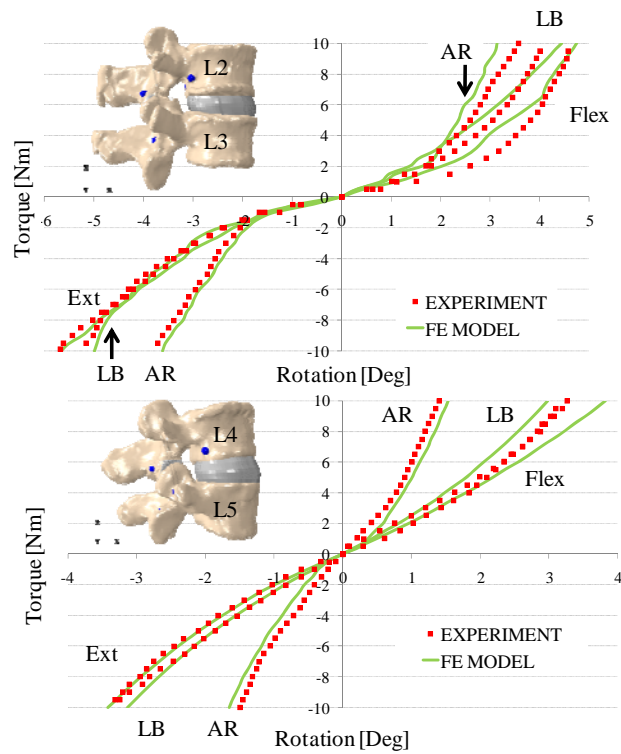


Figure 11. Torque-rotation response for intact spine B - FSU L2-L3 (top) and FSU L4-L5 (bottom).

3.2.3 Range of Motion at the End of the Loading Cycle and RMSE

For comparison, the resulting range of motion or amount of rotation corresponding to the 10 N-m of loading for the intact FSU cases is summarized in Table 5 for the model and experiment. Lastly, root mean squared errors (RMSE) were computed over the torque-rotation curves for each loading degree of freedom. RMSE for all loading cases across various FSUs was between 0.05 and 0.37° with the average being in the range of 0.12 to 0.24°.

Table 5: Range of motion (rotation) with RMSE.

	L2-L3						L4-L5					
	Spine A			Spine B			Spine A			Spine B		
	Exp (deg)	FE (deg)	RMSE (deg)	Exp (deg)	FE (deg)	RMSE (deg)	Exp (deg)	FE (deg)	RMSE (deg)	Exp (deg)	FE (deg)	RMSE (deg)
Flex	4.72	4.68	0.15	5.66	4.75	0.37	8.51	8.87	0.15	3.29	3.82	0.29
Ext	3.40	3.45	0.10	5.28	4.88	0.13	6.52	6.58	0.08	3.43	3.41	0.17
Left LB	3.68	3.62	0.05	5.68	5.67	0.16	4.80	4.65	0.22	3.50	3.13	0.26
Right LB	3.57	3.41	0.10	4.10	4.44	0.29	4.48	4.72	0.25	3.25	2.99	0.26
Left AR	1.94	1.98	0.10	3.58	3.15	0.28	1.78	1.76	0.08	1.40	1.54	0.13
Right AR	2.27	2.15	0.05	3.89	3.61	0.16	1.88	1.84	0.18	1.51	1.65	0.14

3.2.4 Change in Center of Rotation for Various FSUs

The instant center of rotation (ICR) for the overall motion during flexion-extension is shown for the Spine B L4-L5 FSU with varying resection configurations and fully intact in Figure 12. Points A through E configurations are as follows: A=Disc only, B=Disc and facet cartilages only, C=Intact FSU without SSL, ISL and PLL, D=Intact FSU without SSL and ISL, E=Intact FSU. During flexion and extension, it was observed that the ICR of the intact FSU (E) was posterior compared to the other sectioned configurations.

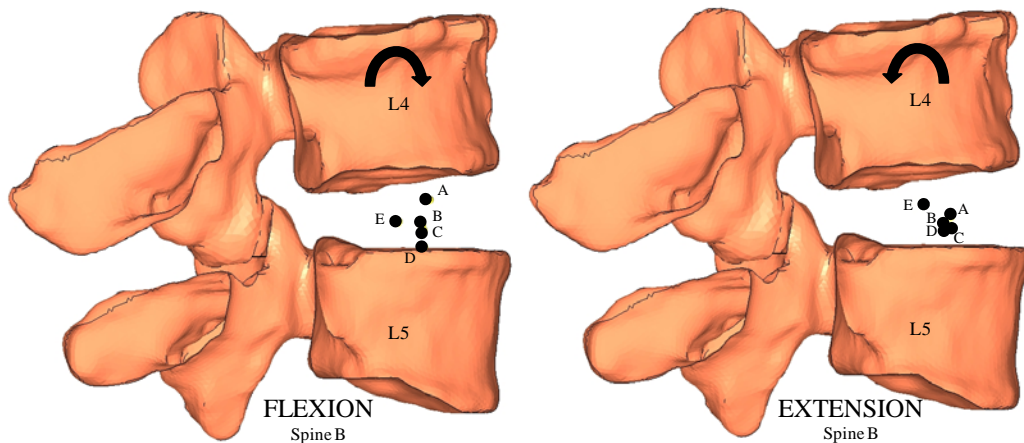


Figure 12. Change in COR: A=disc only, B=disc and facet cartilages only, C=intact FSU without SSL, ISL and PLL, D=intact FSU without SSL and ISL, E=intact FSU.

3.3 Intact Multisegmental Analysis

Spine A and Spine B multisegmental FE models were calibrated for pure moment cases. Comparison of the predicted and experimental torque-rotation curves for Spine A at levels L1-L2, L2-L3, L3-L4, and L4-L5 are presented in Figure 13 for flexion-extension with follower load. The image to the right of each curve indicates the FSU level or whole spine being evaluated. The flexion-extension analyses included a 450N follower load applied along a manually optimized path that maintained intersegmental rotation as close as possible to zero at the end of follower load application. In general, the predicted curves compared well with the experimental behavior. The model predictions tended to match or err with slightly stiffer behavior. Similar evaluations were performed for lateral bend and axial rotation with similar results. Similar evaluations were also performed for Spine B.

As a measure of predictive capability, the model, calibrated with the single degree of freedom analyses, predicted the experimental behavior for a combined flexion (7Nm) and lateral bending (7Nm) loading conditions. The model predictions were within 0.15° of the experimental data and exhibited stiffer torque-rotation behavior.

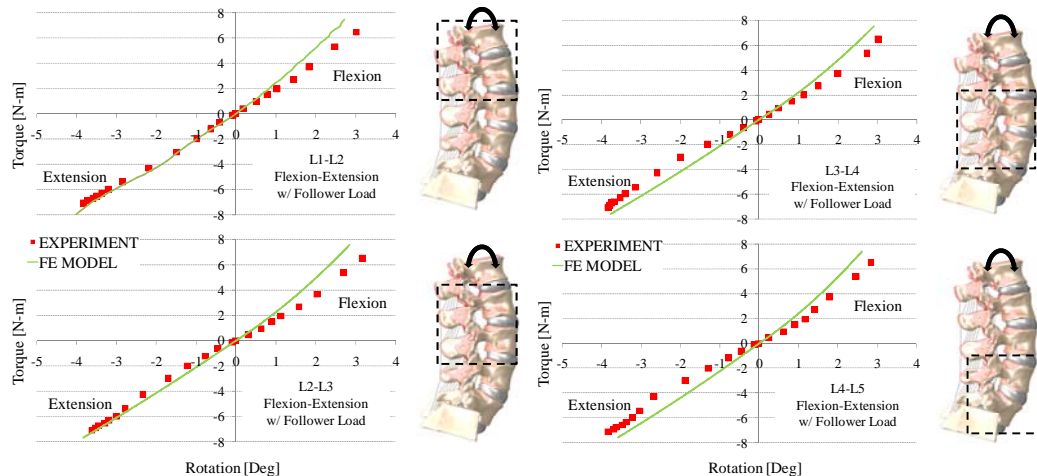


Figure 13. Spine A, torque-rotation response of intact flexion-extension motion with follower load at levels L1-L2, L2-L3, L3-L4, and L4-L5.

4. Discussion and Conclusion

The purpose of this study was to create calibrated FE models of the human lumbosacral spines (FSU and multisegmental) using *in vitro* subject-specific scan and experimental testing data. Patient-specific FE model validation provides improved realism over validation to literature data by considering subject-specific anatomical representations and mechanical behavior. This study utilized a rigorous stepwise structure addition process and applied optimization at each step to match model response to the experimental protocol. The process ensures that the contribution of each structure is appropriately represented in the various degrees of freedom. This is especially relevant for evaluations of implants, as structures are often resected as part of the surgical procedures. By appropriately capturing the contribution of each structure, engineers and designers

can have greater confidence that the instrumented evaluations are appropriately characterizing the contributions of the implant and structures.

A further application of optimization is the development of a computationally efficient model based on a simulated mechanical constraint representation to dramatically reduce analysis times. The improved efficiency of the models will facilitate clinical and design phase assessments, and musculoskeletal modeling studies. It can also allow for probabilistic studies to study model input parameters such as properties of nucleus, annulus and facet, ligament stiffness and reference strain using Isight.

5. References

1. Chazal, J., Tanguy, A., Bourges, M., Gaurel, G., Escande, G., Guillot, M., "Biomechanical properties of spinal ligaments and a histological study of the supraspinal ligament in traction," J Biomech 18, 167-176, 1985.
2. Fujita, Y., Duncan, N.A., Lotz, J.C., "Radial tensile properties of the lumbar annulus fibrosus are site and degeneration dependent", J Orthop Res 15, 814-819, 1997.
3. Guerin, H.L., Elliott, D.M., "Quantifying the contributions of structure to annulus fibrosus mechanical function using a nonlinear, anisotropic, hyperelastic model", J Orthop Res 25, 508-516, 2007.
4. Heuer, F., Schmidt, H., Klezl, Z., Claes, L., Wilke, H.J., "Stepwise reduction of functional spinal structures increase range of motion and change lordosis angle", J Biomech 40, 271-280, 2007.
5. Moramarco, V., Perez del Palomar, A., Pappalettere, C., Doblare, M., "An accurate validation of a computational model of a human lumbosacral segment", J Biomech 43, 334-342.
6. Oxland, T.R., Panjabi, M.M., Southern, E.P., Duranceau, J.S., "An anatomic basis for spinal instability: a porcine trauma model" J Orthop Res 9, 452-462, 1991.
7. Panjabi, M.M., Greenstein, G., Duranceau, J., Nolte, L.P., "Three-dimensional quantitative morphology of lumbar spinal ligaments", J Spinal Disord 4, 54-62, 1991.
8. Panjabi, M.M., White, A.A., 3rd, Johnson, R.M., "Cervical spine mechanics as a function of transection of components", J Biomech 8, 327-336, 1975.
9. Pintar, F.A., Yoganandan, N., Myers, T., Elhagediab, A., Sances, A., Jr., "Biomechanical properties of human lumbar spine ligaments", J Biomech 25, 1351-1356, 1992.
10. Rohlmann, A., Neller, S., Bergmann, G., Graichen, F., Claes, L., Wilke, H.J., "Effect of an internal fixator and a bone graft on intersegmental spinal motion and intradiscal pressure in the adjacent regions", Eur Spine J 10, 301-308, 2001.
11. Wilke, H.J., Wolf, S., Claes, L.E., Arand, M., Wiesend, A., "Stability increase of the lumbar spine with different muscle groups A biomechanical in vitro study", Spine 20, 192-198, 1995.
12. Wilson, D.C., Niosi, C.A., Zhu, Q.A., Oxland, T.R., Wilson, D.R., "Accuracy and repeatability of a new method for measuring facet loads in the lumbar spine", J Biomech 39, 348-353, 2006.
13. Zander, T., Rohlmann, A., Bergmann, G., "Influence of ligament stiffness on the mechanical behavior of a functional spinal unit", J Biomech 37, 1107-1111, 2004.